SECOND EUROPEAN CONFERENCE ON EARTHQUAKE ENGINEERING
AND SEISMOLOGY, ISTANBUL AUG. 25-29, 2014

THE DYNAMICS OF A PUSHING AND QUICK RELEASE DEVICE FOR DYNAMIC TESTING OF SEISMIC ISOLATED BUILDINGS

Giuseppe OLIVETO[1] and Athanasios A. MARKOU[2]

ABSTRACT

A pushing and quick-release device was designed, built and applied for the dynamic testing of a four-story reinforced concrete building in the town of Solarino in south-east Sicily seismically retrofitted by hybrid base isolation. The tests were performed in July 2004 and the results have been shown in the literature Oliveto et al. (2004). In March 2013 the same device has been used for the testing of a newly built reinforced concrete building in the town of Augusta also in eastern Sicily. A similar hybrid seismic isolation system to the one in Solarino was used also for the building in Augusta. Preliminary blind studies in preparation of the actual tests were presented at the 10CUEE conference in Japan, Oliveto et al. (2013). The object of the present work is to discuss the dynamics of the pushing and quick release device rather than the performance of the base isolation system. It is believed that the present discussion will provide a better understanding of the behavior of the considered device which might encourage other researchers to use similar devices for full scale dynamic tests of base isolation systems.

INTRODUCTION

In 2003-2004 two four-story reinforced concrete buildings were seismically retrofitted by a Hybrid Base Isolation System (HBIS) in Solarino, Eastern Sicily. One of these two buildings was subjected to free vibration tests in July of 2004. The results of the tests have been discussed in the literature, Oliveto et al., (2004). In March 2013 a new building seismically isolated by HBIS was also subjected to a series of free vibration tests. The building consists of two storeys above the isolation plane and of a smaller third storey. In both cases the loading apparatus for the free vibration tests consisted of a pushing and quick-release device, a reaction wall, a hydraulic jack and a load cell, Fig.1. The purpose of the present work is to study the dynamics of the pushing and quick release device.

DESCRIPTION OF THE PUSHING AND QUICK-RELEASE DEVICE

Ideally the mechanical model for the pushing and quick-release devise is an articulated quadrilateral with a spring connecting two opposite vertices acting as a fuse, Fig.2. The fuse consists of a calibrated rod of high strength steel which undergoes negligible plastic deformation before rupture. The rupture load for the fuse can therefore be pre-determined with sufficient accuracy on the base of the diameter of the cross-section and of the rupture tensile stress for the material. Samples obtained from the same rod can be tested in the laboratory to assure that the rupture load is known in advance with sufficient

[1] Professor, University of Catania, Catania, golive@dica.unict.it
[2] PhD student, Aristotle University of Thessaloniki, Thessaloniki, athanasiosmarkou@gmail.com

accuracy. The rupture strength of the fuse can be related to the maximum load applied by the device just before release by a simple geometrical relationship:

$$P = S \cdot \tan\alpha = m \cdot S \tag{1}$$

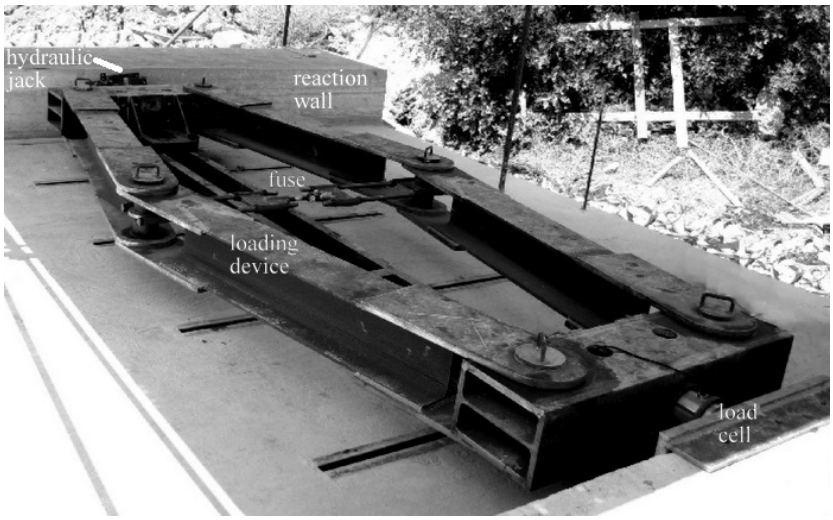

Figure 1. Pushing and quick release device prototype (Oliveto et al., 2004).

where P is the pushing force applied by the device, S is rupture strength of the fuse and α is the angle that any member of the articulated mechanism forms with the loading axis. Eq.(1) shows that there are two ways of increasing the pushing force; either by increasing the strength of the fuse or by increasing the angle α. By adjusting S and α an ample set of pushing loads can be obtained, according to the needs of the tests that must be performed.

For construction and application reasons two heads have been provided to the device, one head where the loading jack is applied and the other head where the load applied to the structure is measured through a load cell. In this way the two end hinges of the quadrilateral mechanism are each duplicated, separating the left arm and the right arm of the device which then appears as is shown in Fig.3. The two heads of the device can move on a rail so that, when the fuse breaks and the strain energy stored in the device is suddenly released, the device opens until all the kinetic energy is dissipated by friction in the articulations and on the rail.

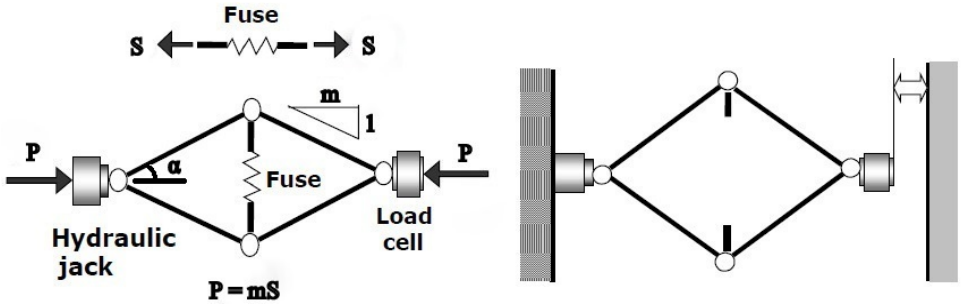

Figure 2. Idealized model of pushing and quick release device (Oliveto et al., 2004).

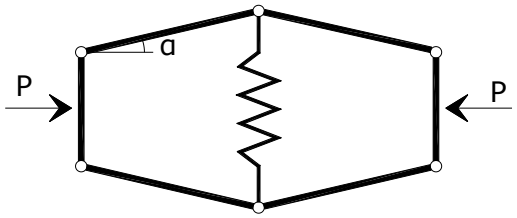

Figure 3. Sketch of the pushing and quick-release device as built.

CONSTRUCTION DETAILS OF PUSHING AND QUICK RELEASE DEVICE

The elements which constitute the pushing and quick release device are labeled in Fig.4 and are described in Table.1. The 4 elements labeled (01) are made of HEB 300 steel beams. The 2 front and back ends (02) are made of HEB 400 steel beams welded to two steel plates 30x350x1500. As it may be seen from Fig.1, the cross-section of element (02) is triple-connected by construction. Element (03), shown in detail in Fig.5, is specially constructed to accommodate the fuse. Elements (04) are the supports of the pushing and quick-release device which allow the same to move on the rail (06). The device is completed by six hinge-pins labeled (05) in Fig.4. The side view in Fig.4 shows the device and the rail on which it moves during the pushing phase and the subsequent release phase.

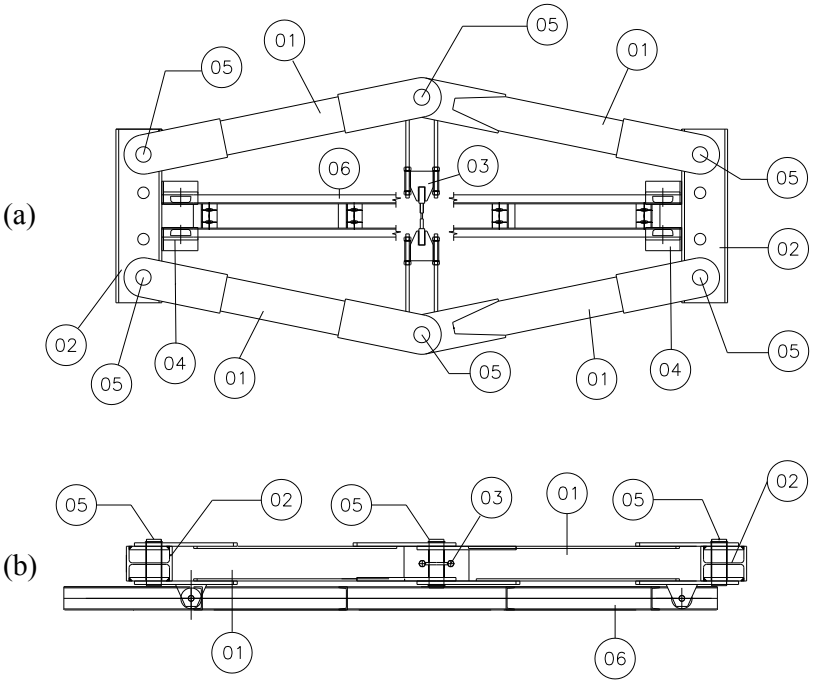

Figure 4. (a) Plan and (b) side view of pushing and quick-release device

Table 1. Components of the quick-release device (Fig.4)

Labels	Description	Number of items
01	Main Beams – HEB 300	4
02	Head Beams – HEB 400	2
03	Fuse – Bars Φ30	2
04	Translational Apparatus	4
05	Hinge Pins – Φ130	6
06	Rails – UPN 200	2

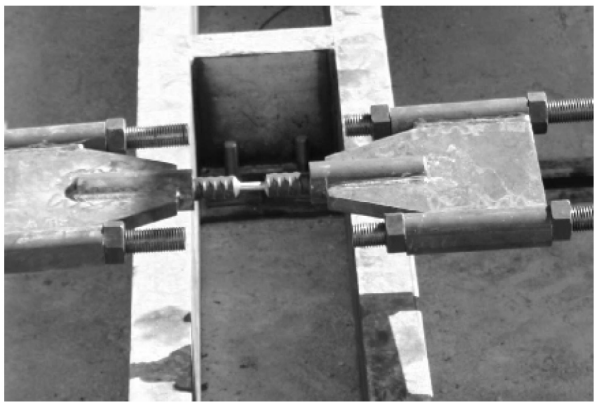

Figure 5. Calibrated high-strength steel rod acting as a fuse in its lodging.

MECHANICAL MODELS OF THE PUSHING AND QUICK-RELEASE DEVICE

Two simple mechanical models have been used to describe the dynamic behaviour of the device during the release phase. The first one is based on lumped masses to describe the inertial behaviour and on a Coulomb friction model to describe the energy dissipation. The second model is based on distributed masses to describe the inertial behaviour and the same Coulomb friction model to describe energy dissipation. The sketch in Fig.6 shows the device during the pushing phase. It is assumed that the system is rigid and that its configuration changes little under load apart from a rigid translation corresponding to the stroke of the jack and to the displacement of the building. The main components of the idealized model are the 4 elements E_1 of length L_1 and mass m_1, the 2 elements E_2 of length L_2 and mass m_2, the 2 elements E_3 of length L_3 and of negligible mass, and the element E_4 of length L_4 and of negligible mass corresponding to the fuse. It should be noticed that the system has only one degree of freedom because the elements E_2 can only move on the longitudinal rail while transverse displacements and rotations are prevented. The relevant geometrical and material data about each of the components previously described are given in Table.2. The internal forces in the components of the pushing and quick-release device, which are given in Table.3, depend on the applied load P and on the assumed configuration defined by the angle α_0. The internal forces given in Table.3 and the geometrical and material properties provided in Table.2 can be used to calculate the elastic strain energy stored in the device for the given configuration and applied load through the formula:

$$E_S = 4 \cdot \frac{N_1^2 \cdot L_1}{2 \cdot E \cdot A_1} + 2 \cdot \frac{N_2^2 \cdot L_2}{2 \cdot E \cdot A_2} + 2 \cdot \frac{N_3^2 \cdot L_3}{2 \cdot E \cdot A_3} + \frac{N_4^2 \cdot L_4}{2 \cdot E \cdot A_4} + 2 \cdot \frac{M_2^2 \cdot L_2}{6 \cdot E \cdot I_2} + 2 \cdot \frac{V_2^2 \cdot L_2}{2 \cdot \kappa \cdot G \cdot A_2} \qquad (2)$$

Table 2. Geometrical and material data for device components.

Elements	Mass m (tons)	Length L (m)	Cross sectional area $A \cdot 10^6$ (m^2)	Second moment of area $I \cdot 10^9$ (m^4)	Elastic Modulus E (MPa)	Shear Modulus G (MPa)	Shear correction factor κ
E_1	0.57678	2.477	14910	-	205970	80000	0.20
E_2	0.53169	1.062	40780	791175			
E_3	-	0.561	1414	-			
E_4	-	0.433	531	-			

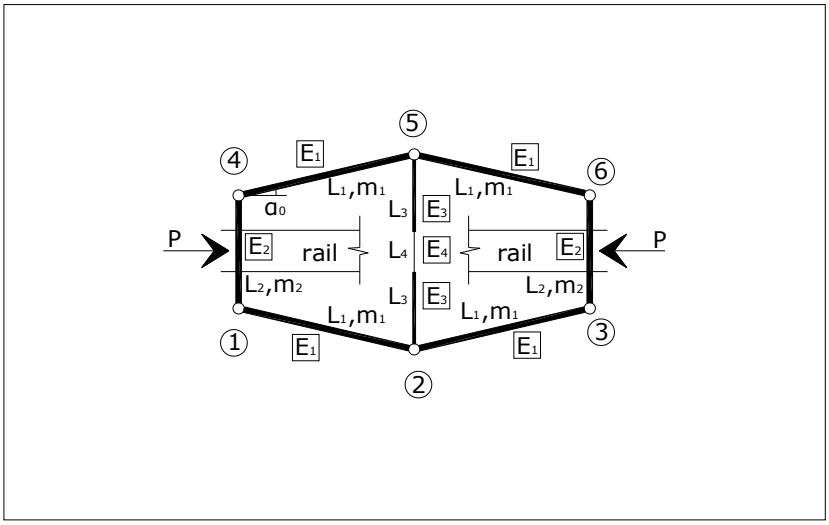

Figure 6. Sketch of the pushing and quick release device with main components.

Table 3. Internal forces in device components.

Elements	Axial Force	Shear Force	Bending Moment (midspan)
E_1	$N_1 = \dfrac{P}{2 \cdot \cos(\alpha_0)}$	-	-
E_2	$N_2 = \dfrac{P \cdot \tan(\alpha_0)}{2}$	$V_2 = \dfrac{P}{2}$	$M_2 = \dfrac{P \cdot L_2}{4}$
E_3	$N_3 = P \cdot \tan(\alpha_0)$	-	-
E_4	$N_3 = P \cdot \tan(\alpha_0)$	-	-

Model kinematics

The model kinematics in the release phase is shown in Fig.7. Because the device is symmetrical, upon release of the load, when the fuse breaks, the front-end in contact with the building and the back-end in contact with the reaction wall retract symmetrically as shown in the figure. The time is counted starting from the instant when the load is released and at any time t the above described retraction is indicated by $u(t)$. This retraction occurs simultaneously with a change (increase) of the configuration angle which from α_0 becomes $\alpha(t)$. The opening of the device determines an outward displacement of the central hinges of the device denoted by $v(t)$. Both $u(t)$ and $v(t)$ are related to the configuration angle $\alpha(t)$ through simple geometric relationships. These are given in Table.4 together with the corresponding expressions for velocities and accelerations.

Table 4. Kinematic relationships for displacement, velocity and acceleration.

$u(t)$	$L_1 \cdot (\cos\alpha_0 - \cos\alpha(t))$
$v(t)$	$L_1 \cdot (\sin\alpha(t) - \sin\alpha_0)$
$\dot{u}(t)$	$L_1 \cdot \sin\alpha(t) \cdot \dot{\alpha}(t)$
$\dot{v}(t)$	$L_1 \cdot \cos\alpha(t) \cdot \dot{\alpha}(t)$
$\ddot{u}(t)$	$L_1 \cdot (\cos\alpha(t) \cdot \dot{\alpha}(t)^2 + \sin\alpha(t) \cdot \ddot{\alpha}(t))$
$\ddot{v}(t)$	$L_1 \cdot (-\sin\alpha(t) \cdot \dot{\alpha}(t)^2 + \cos\alpha(t) \cdot \ddot{\alpha}(t))$

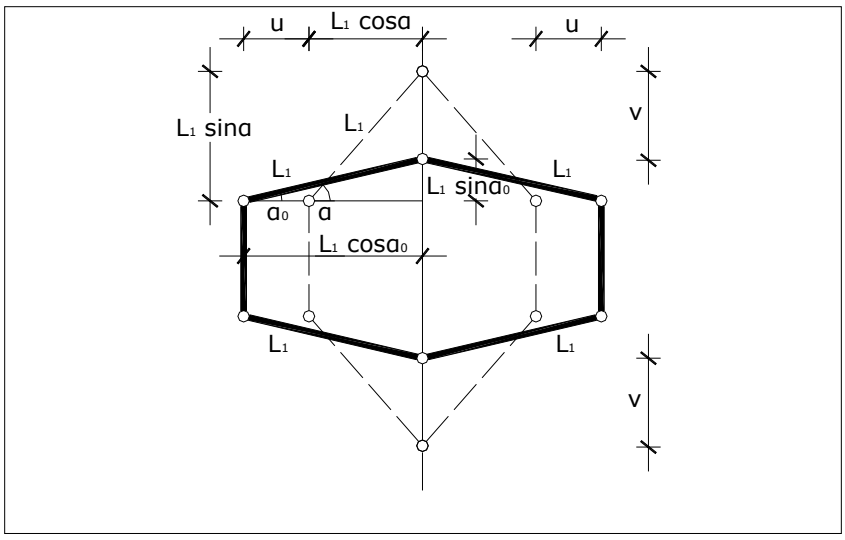

Figure 7. Kinematics of the device in the release phase.

Lumped mass model

With reference to the component distribution shown in Fig.6 and to the masses given in Table.2 the lumped mass model shown in Fig.8 has been constructed. The system of inertia and friction forces

compatible with the kinematic mechanism of Fig.7 is shown in Fig. 9. Application of the principle of virtual displacements leads to the following equation of motion:

$$\ddot{\alpha}(t)+\dot{\alpha}^2(t)\frac{\sin\alpha(t)\cdot\cos\alpha(t)}{\left(\frac{m_1}{m_2}+\sin^2\alpha(t)\right)}+\frac{2\cdot F_2\cdot\sin\alpha(t)+F_1\cdot\cos\alpha(t)}{m_2\cdot L_1\cdot\left(\frac{m_1}{m_2}+\sin^2\alpha(t)\right)}\cdot sign(\dot{\alpha}(t))=0 \tag{3}$$

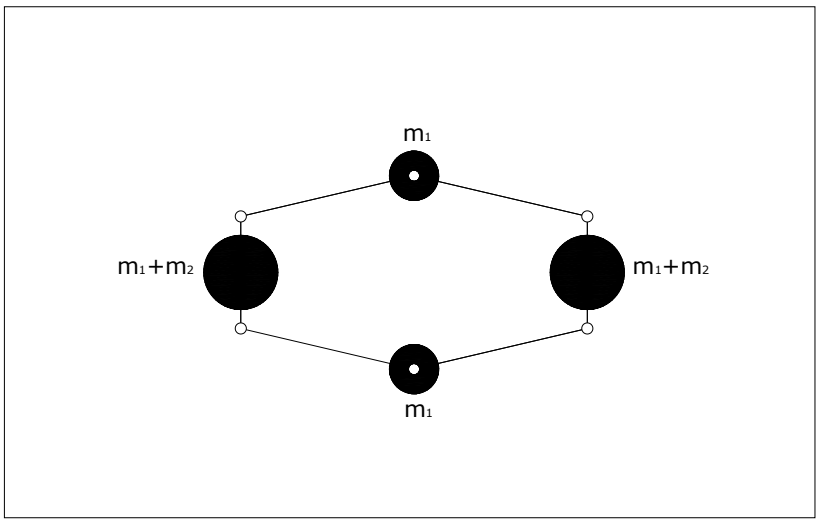

Figure 8. Distribution of masses of lumped mass model.

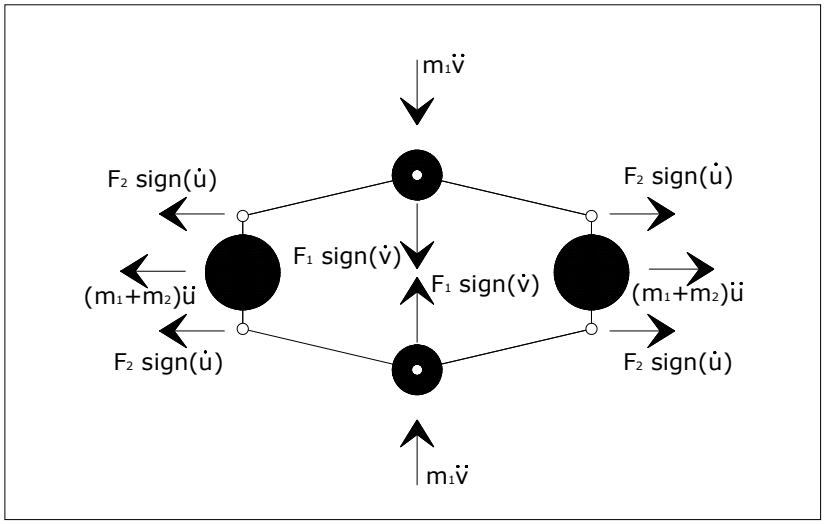

Figure 9. Inertia and friction forces of lumped mass model.

Distributed mass model

A more accurate model can be obtained considering the actual distribution of the masses of the system components. Because elements E_3 and E_4 are of negligible mass and elements E_2 move as subjected to a rigid translation, the only elements for which the distribution of mass is relevant are element E_1. With reference to Fig.10, the kinematic of a cross-section at position z can be described by a displacement $x(z,t)$ parallel to $u(t)$ and a displacement $y(z,t)$ parallel to $v(t)$. The analytical expressions for displacements, velocities and accelerations as function of the position of the cross-section in elements E_1 are given in Table.5. By accounting for the distributed inertia forces shown in Fig.11, application of the principle of virtual displacements leads to the following equation of motion:

$$\ddot{\alpha}(t)+\dot{\alpha}^2(t)\frac{\sin\alpha(t)\cdot\cos\alpha(t)}{\left(\frac{2}{3}\cdot\frac{m_1}{m_2}+\sin^2\alpha(t)\right)}+\frac{2\cdot F_2\cdot\sin\alpha(t)+F_1\cdot\cos\alpha(t)}{m_2\cdot L_1\cdot\left(\frac{2}{3}\cdot\frac{m_1}{m_2}+\sin^2\alpha(t)\right)}\cdot sign(\dot{\alpha}(t))=0 \qquad (4)$$

Comparison of the equations of motion Eq.(3) and Eq.(4) shows that the two are structurally similar and differ only for a dimensionless factor multiplying a mass ratio in two variable coefficients of the equations. Therefore the same solution method will be applicable to both equations.

Table 5. Kinematic relationships for displacement, velocity and acceleration of E_1.

$x(z)$	$y(z)$	$\dot{x}(z)$	$\dot{y}(z)$	$\ddot{x}(z)$	$\ddot{y}(z)$
$u(t)\cdot\frac{z}{L_1}$	$v(t)\cdot\left(1-\frac{z}{L_1}\right)$	$\dot{u}(t)\cdot\frac{z}{L_1}$	$\dot{v}(t)\cdot\left(1-\frac{z}{L_1}\right)$	$\ddot{u}(t)\cdot\frac{z}{L_1}$	$\ddot{v}(t)\cdot\left(1-\frac{z}{L_1}\right)$

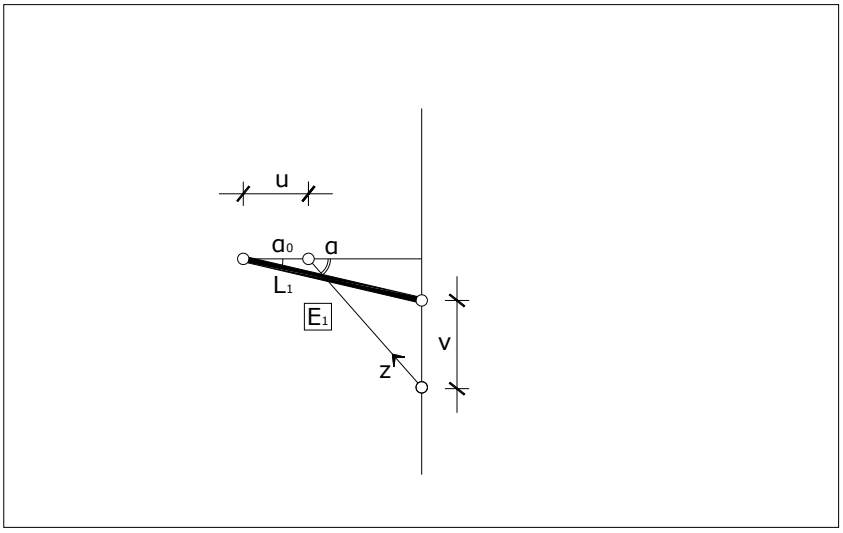

Figure 10. Element E_1 of the system.

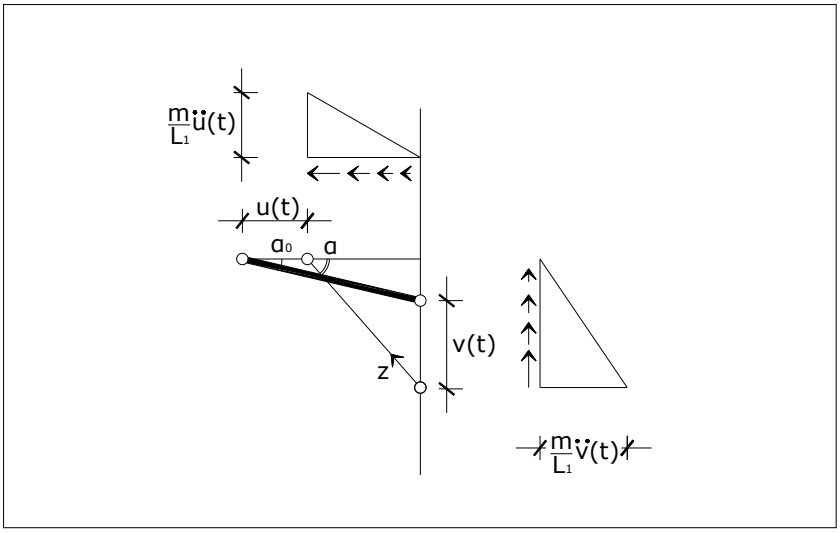

Figure 11. Inertia forces of element E_1 of the distributed mass model.

INITIAL CONDITIONS FOR THE RELEASE PHASE

When the fuse breaks the stable systems becomes a mechanism and the stored elastic strain energy transforms instantaneously into kinetic energy. It is a simple exercise to show that the general expression for the kinetic energy is:

$$E_K(t) = m_2 \cdot L_1^2 \cdot \left[c \cdot \frac{m_1}{m_2} + \sin^2 \alpha(t) \right] \cdot \dot{\alpha}(t)^2 \tag{5}$$

where the parameter c takes the value 1 for the lumped mass model and 2/3 for the distributed mass model. Because the equations of motion for the lumped mass model and for the distributed mass model are both second order ordinary differential equations, two initial conditions are necessary in order to provide a unique solution to the problem. The first condition can be provided in terms of configuration angle which must be equal to the angle chosen for the pushing phase. The second condition must be given in terms of initial velocity which can be obtained by equating the initial kinetic energy to the stored elastic energy an instant before release. Therefore the two initial conditions can be formulated as follows:

$$\alpha(0) = \alpha_0; \qquad \dot{\alpha}(0) = \dot{\alpha}_0 = \sqrt{\frac{E_S}{m_2 \cdot L_1^2 \cdot \left[c \cdot \frac{m_1}{m_2} + \sin^2 \alpha_0 \right]}} \tag{6}$$

DISSIPATED ENERGY AND FINAL CONFIGURATION

Given the considered system based on the Coulomb Friction Model (CFM), the dissipated energy at any time is a function of the current configuration $\alpha(t)$ and of the initial configurations α_0. In terms of the friction forces specified in Fig.9, the dissipated energy corresponding to the configuration $\alpha(t)$ takes the following expression:

$$W_F = 2 \cdot F_1 \cdot L_1 \cdot \left(\sin \alpha(t) - \sin \alpha_0 \right) + 4 \cdot F_2 \cdot L_1 \cdot \left(\cos \alpha_0 - \cos \alpha(t) \right) \tag{7}$$

During the release phase the total energy of the system is provided by its kinetic energy which takes expression of Eq.(5). The motion of the system stops when the kinetic energy vanishes and this occurs when the initial potential energy has been totally dissipated. This conjecture yields the following non-linear algebraic equation for the evaluation of the final configuration angle α_F taken by the device after release.

$$E_S = 2 \cdot F_1 \cdot L_1 \cdot \left(\sin \alpha_F - \sin \alpha_0 \right) + 4 \cdot F_2 \cdot L_1 \cdot \left(\cos \alpha_0 - \cos \alpha_F \right) \tag{8}$$

Figure 12.(a) Device configuration in the pushing phase and (b) final configuration upon release.

The two pictures in Fig.12 show the pushing and quick-release device in the initial configuration α_0 before a test and in the final configuration α_F after the test.

SOLUTION ALGORITHM

A simple and efficient algorithm for the solution of the non-linear equations of motion Eq.(3) and Eq.(4) is provided in Table.6. The algorithm is based on the fact that the equation of motion to be resolved is linear in the angular acceleration term; therefore the angular acceleration at the end of a time step can be evaluated by solving the equation of motion if the angular velocity and the position angle at the end of the step are known. The angular velocity at end of the step is provided by its first order Taylor expansion at the beginning of the step while the position angle is evaluated by using the central difference mid-point rule for the velocity.

The performance of the algorithm has been checked against the MATLAB ode45 solver based on the Runge-Kutta method. The second order differential equation was transformed in a system of two first order differential equations before application of ode45. The obtained results were coincident with those of the proposed algorithm. A more definite check on the accuracy of the proposed algorithm has been obtained by the following energy based solution. For any position angle α the kinetic energy of the system is provided by Eq.(5) which is equal to the difference between the initial potential energy E_S and the dissipated energy $W_F(\alpha)$:

$$E_K(t) = m_2 \cdot L_1^2 \cdot \left[c \cdot \frac{m_1}{m_2} + \sin^2 \alpha(t) \right] \cdot \dot{\alpha}(t)^2 = E_S - W_F\left(\alpha(t)\right) \tag{9}$$

Eq.(9) can be solved for the angular velocity $\dot{\alpha}(t)$ providing a state plot $(\alpha(t), \dot{\alpha}(t))$ which can be used as a test for the accuracy of the proposed algorithm. The mapping with time can then be established by solving the first order differential equation:

$$\dot{\alpha}(t) = \sqrt{\frac{E_S - W_F\left(\alpha(t)\right)}{m_2 \cdot L_1^2 \cdot \left[c \cdot \frac{m_1}{m_2} + \sin^2 \alpha(t) \right]}} \tag{10}$$

Table 6. Solution algorithm.

$\dot{\alpha}_k = \dot{\alpha}_{k-1} + \ddot{\alpha}_{k-1} \cdot \Delta t$
$a_k = a_{k-1} + \frac{\dot{a}_k + \dot{a}_{k-1}}{2} \cdot \Delta t$
$\ddot{\alpha}_k(t) = -\dot{\alpha}_k^2(t) \cdot \frac{\sin\alpha_k(t) \cdot \cos\alpha_k(t)}{\left(c \cdot \frac{m_1}{m_2} + \sin^2 \alpha_k(t) \right)} - \frac{2 \cdot F_2 \cdot \sin\alpha_k(t) + F_1 \cdot \cos\alpha_k(t)}{m_2 \cdot L_1 \cdot \left(c \cdot \frac{m_1}{m_2} + \sin^2 \alpha_k(t) \right)} \cdot sign(\dot{\alpha}_k(t))$

IDENTIFICATION OF FRICTION FORCES

For the identification of the friction forces F_1 and F_2 the available information is what can be gathered from Fig.12, that is the initial configuration angle α_0, the final configuration angle α_F, and the time t_F required for passing from the initial to the final configuration. Also known is the final pushing force P before release and consequently the potential energy E_S immediately before release.

First it should be noticed that the friction forces F_1 and F_2 are not independent because they must satisfy Eq.(8). Furthermore each one of them can at most vanish, while negative values are not admissible. Upper bounds for each of them can be found on the basis that when the other vanishes the remaining positive one can take at most the value that annuls the kinetic energy in the final configuration, that is:

$$0 \le F_1 \le F_1^* \qquad F_1^* = \frac{E_S}{2 \cdot L_1 \cdot (\sin \alpha_F - \sin \alpha_0)} \tag{11}$$

$$0 \le F_2 \le F_2^* \qquad F_2^* = \frac{E_S}{4 \cdot L_1 \cdot (\cos \alpha_0 - \cos \alpha_F)} \tag{12}$$

Finally the relationship between the two friction forces may be written as follows:

$$F_2 = F_2^* \left(1 - \frac{F_1}{F_1^*} \right) \tag{13}$$

The values of the parameters measured during the test and of those estimated from Fig.12 are given in the first five columns of Table.7. In the sixth column is given the parameter that accounts for distributed mass, while the identified friction forces are given in the last two columns.

Table 7. Estimated and identified parameters.

P (kN)	α_0 (rad)	α_F (rad)	E_S (kNm)	t_F (sec)	c	F_1 (kN)	F_2 (kN)
1598	0.2000	0.7378	2.90	1.05	2/3	0.4056	0.8154

The identification has been pursued by using the estimated and measured parameters in the solution algorithm and by assigning tentative values to the friction force parameter F_2 / F_2^* in the range between 0 and 1. The procedure has been considered completed when the final time produced by the solution algorithm has resulted coincident with the time t_F measured during the test. The identified friction forces appear to be reasonable in view of the distribution of the dissipation sources present in the device.

RESULTS

The results produced by the solution algorithm in the final stage of the identification process are shown in Fig.13. The position angle is shown in Fig.13(a) as a function of time; it is evident how the final configuration of the device is reached in the time measured during the test. It may be noticed how the final configuration is approached with a slowing speed. This is confirmed by the graph of the angular velocity shown in Fig.13(b). It may be worth noticing that the velocity vanishes when the final configuration is achieved. The graph in Fig.13(c) shows the angular acceleration as a function of time; it may be interesting to notice that the acceleration initially increases reaching a maximum and then decreases up to the time when the velocity vanishes. At that time it drops to 0 as simultaneously do the friction forces which balance the inertia forces. Finally in Fig.13(d) the energy balance is shown; it may be seen that the kinetic energy diminishes as the dissipated energy increases. However the sum of the kinetic and dissipated energy is always equal to the initial potential energy stored in the device. Fig.14(a) shows the linear displacement $u(t)$ along the longitudinal axis of the device and the linear displacement $v(t)$ along its transverse axis, while Fig.14(b) shows the corresponding velocities. It may

be noticed how the transverse displacement, corresponding to the opening of the device is much larger than the longitudinal displacement. The graph for the velocity shows a maximum velocity in the range between 2 and 3 m/s and a maximum longitudinal velocity of the order of 1 m/s. Finally in Fig.15 the state diagram $(\alpha(t),\dot{\alpha}(t))$ is shown. The response obtained by the numerical solution algorithm is exactly superimposed to the analytical solution provided by Eq.(10).

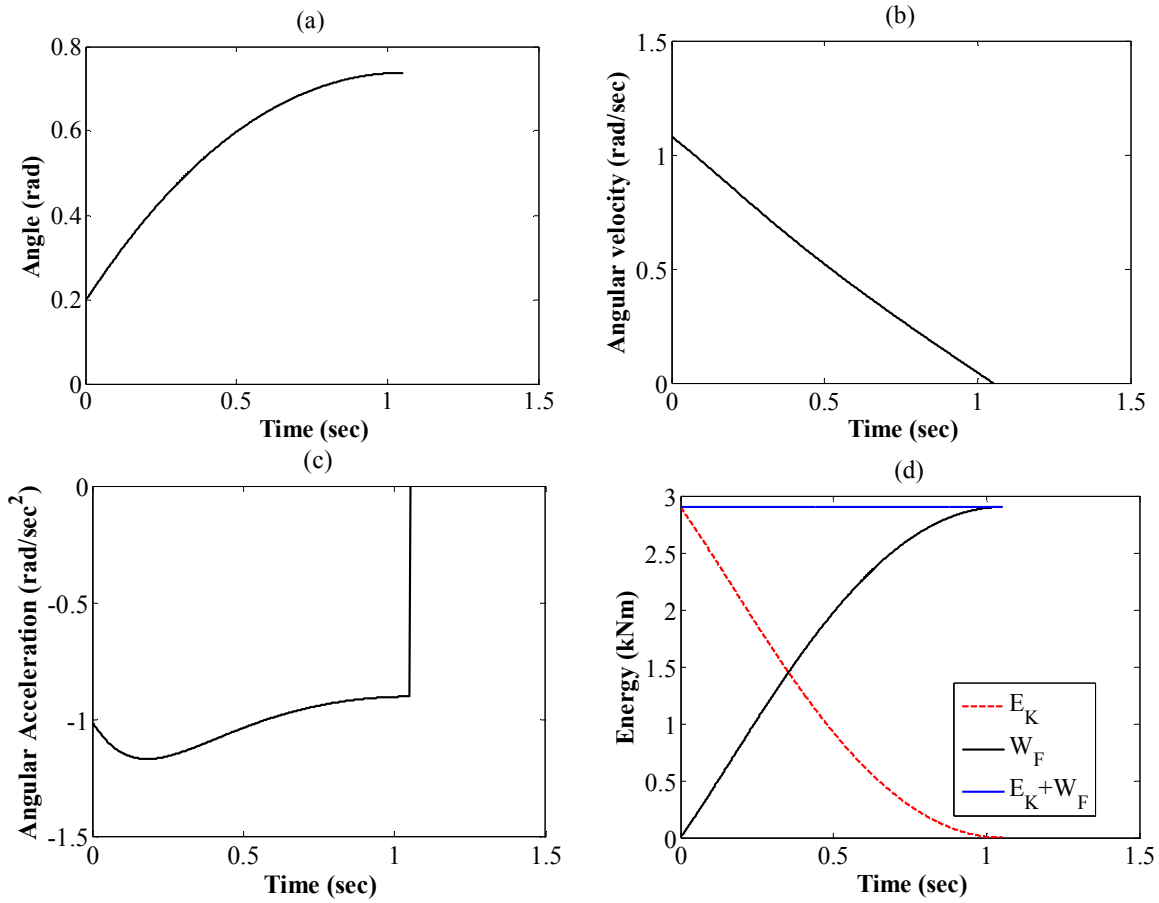

Figure 13. Response for distributed mass model; (a) position angle, (b) angular velocity, (c) angular acceleration, (d) energy balance.

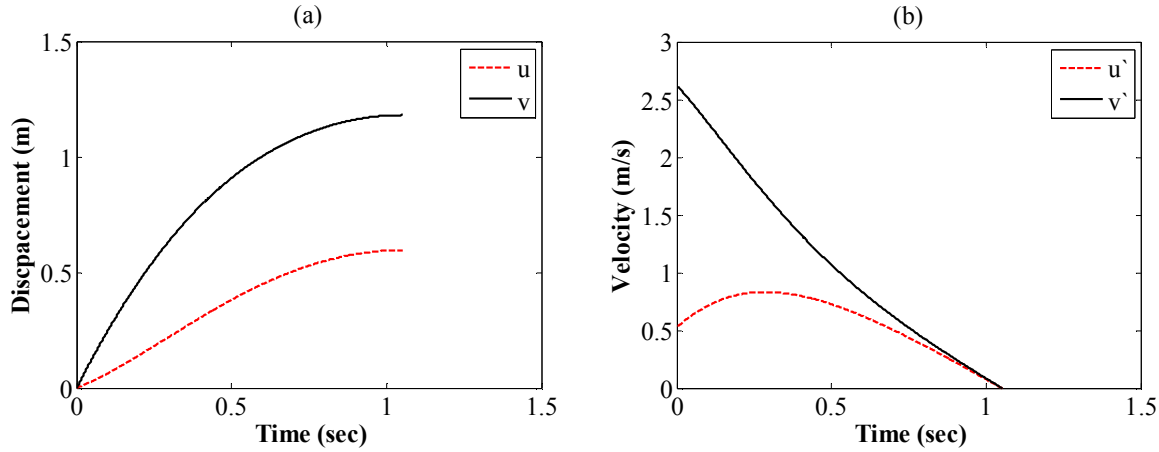

Figure14. Linear displacement and velocity response.

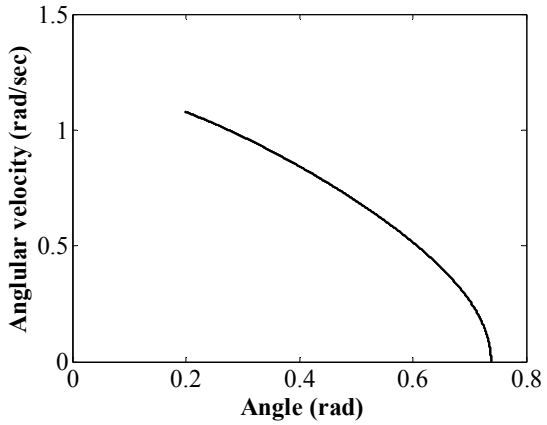

Figure 15. Response state diagram for device.

CONCLUSIONS

A dynamical model for the behaviour of a pushing and quick-release device has been presented. The inertial behaviour has been described by a lumped mass model and by a distributed mass model. The resulting equations of motion are structurally similar in the two cases and the difference is only in a numerical coefficient. In the applications only the distributed mass model has been used because it has been felt to better describe the actual behaviour. Because the present study had not been planned at the time of the tests, the available information for the identification of the friction forces was scanty and mainly reduced to what could be gathered from Fig.12. The model identification would have been much more reliable if displacements and accelerations on the device had been measured during the tests. However the use of the available information has allowed to develop a model that describes in a realistic way the behaviour of the device during the tests. The numerical algorithm developed for the integration of the highly non-linear equation of motion has proved to be robust and efficient with obtained results totally superimposed to the analytical ones for the state diagram shown in Fig.15. This study has been carried out with the intention to attract the attention of the researchers and practitioners to the use of this simple device for full scale field testing of base isolated buildings. The device presented in this work has been used so far to test two base isolated buildings in Eastern Sicily. The friction forces developed in the hinges and on the wheels of the translation apparatus of the device have been described by a simple Coulomb model. It may be interesting to see in future experiments how the friction forces are influenced by the amplitude of the applied load and by the initial configuration angle.

ACKNOWNLEDGEMENTS

This work was performed with the financial support of RELUIS (Italian National Network of University Earthquake Engineering Laboratories), “Project D.P.C. – RELUIS 2014-2016, WP1”. Athanasios Markou was able to participate in this work due to the “Anastasios Anastasiadis” grant of the Aristotle University of Thessaloniki.

REFERENCES

Oliveto G, Granata M, Buda G, Sciacca P (2004) “Preliminary results from full scale free vibration tests on a four story reinforced concrete building after seismic rehabilitation by base isolation”, *Proceedings of the JSSI 10th Anniversary Symposium on Performance of Response Controlled Buildings*, Yokohama, Japan, 17-19 November, 1303-1316

Oliveto G, Athanasiou A, Granata M (2013) “Blind simulation of full scale free vibration tests on a three story base isolated building”, *Proceedings of the 10th International Conference on Urban Earthquake Engineering*, Tokyo, Japan, 1-2 March, 1303-1316